CCFE-PR(16)20

J.T. Omotani, F. Militello, L. Easy and N.R. Walkden

The Effects of Shape and Amplitude on the Velocity of Scrape-off Layer Filaments

The Effects of Shape and Amplitude on the Velocity of Scrape-off Layer Filaments

J.T. Omotani[1], F. Militello[1], L. Easy[2;1] and N.R. Walkden[1]

[1]CCFE, Culham Science Centre, Abingdon, Oxon, OX14 3DB, UK
[2]Department of Physics, University of York, Heslington, York YO10 5DD, UK

The effects of shape and amplitude on the velocity of scrape-off layer filaments

JT Omotani[1], F Militello[1], L Easy[2,1], NR Walkden[1]

[1] CCFE, Culham Science Centre, Abingdon, Oxon, OX14 3DB, UK
[2] Department of Physics, University of York, Heslington, York YO10 5DD, UK

E-mail: john.omotani@ccfe.ac.uk

Abstract.

A complete model of the dynamics of scrape-off layer filaments will be rather complex, including temperature evolution, three dimensional geometry and finite Larmor radius effects. However, the basic mechanism of $\boldsymbol{E}\times\boldsymbol{B}$ advection due to electrostatic potential driven by the diamagnetic current can be captured in a much simpler model; a complete understanding of the physics in the simpler model will then aid interpretation of more complex simulations, by allowing the new effects to be disentangled. Here we consider such a simple model, which assumes cold ions and isothermal electrons and is reduced to two dimensions. We derive the scaling with width and amplitude of the velocity of isolated scrape-off layer filaments, allowing for arbitrary elliptical cross-sections, where previously only circular cross-sections have been considered analytically. We also put the scaling with amplitude in a new and more satisfactory form. The analytical results are extensively validated with two dimensional simulations and also compared, with reasonable agreement, to three dimensional simulations having minimal variation parallel to the magnetic field.

Filaments are a prominent feature of the scrape-off layer (SOL) of tokamaks, in L-mode and in H-mode both during and between ELMs[1], and in other magnetised plasmas. They provide a significant component of the particle transport[2], especially in the far SOL, and so may have a strong impact on particle fluxes to the first wall and divertor. Data from gas-puff imaging diagnostics[3] suggests that filaments may sometimes have significantly elliptical (rather than circular) cross-sections. Most of the theoretical work on SOL filaments has been done in simplified, two dimensional models, see [4] and [5] for reviews, but recently there has been an increasing amount of attention given to increasingly realistic models, for example using three dimensional simulations[6–8] or including finite Larmor radius effects[9]. These developments have motivated us to re-examine and extend the earlier analytical work to try to give as complete a physical picture of the two dimensional mechanisms that regulate filament motion as possible, in order to facilitate the interpretation of more complicated models applied to isolated filaments, and ultimately to SOL turbulence simulations[10–12].

Our subject here is the scaling of filament velocity with various parameters of the filament, in the two dimensional limit where parallel variation may be neglected and assuming cold ions and isothermal electrons. In order to be able to make progress analytically we assume that the filaments propagate coherently and steadily, i.e. at constant velocity and without changing their shape. In practice the shape of the filaments does evolve with time (typically 'mushrooming' or 'fingering'[13]), but the steady state value estimates a typical velocity of the filaments. We will see in Section 2 that the calculation corresponds well to the maximum velocity of filaments in simulations. Finite Larmor radius effects may also increase the coherence of filaments[9], and L-mode and inter-ELM filaments are observed experimentally to have small accelerations[1, 14]. This represents the very simplest model that can capture the basic mechanism of filament motion. By characterising quantitatively the basic physical processes driving filament motion in this simple model, we will be able, when analysing more complicated models, to identify the deviations from this behaviour. These deviations can then be ascribed to the extra physics in, for example, three-dimensional or non-isothermal simulations. The aim therefore is to provide a theoretical tool to aid the interpretation of more complicated models, as part of a programme of research building systematically towards models which are both well enough understood to be trusted and also realistic enough to be quantitatively compared to experiment and used predictively for future machines. The particular model we consider contains two principal mechanisms that limit the filament velocity: inertia and sheath currents; viscosity is also present. While inertia is universally present, the sheath current (as modelled here) is only relevant on the assumption that parallel resistivity is small so that parallel currents may reach the sheath unimpeded. Where this assumption is invalid, whether due to cold plasma[15] or interaction with neutrals in the divertor or to large magnetic shear near X-points, different mechanisms will come into play; for some examples see [4]. If it is desired to include other effects, as different closures for the two dimensional equations, we hope that the framework of the calculation provided here will make further additions relatively straightforward.

We present here a calculation of the scaling of the filament velocity allowing arbitrary elliptical cross-sections, which have not previously been considered analytically. We also aim to clarify the physical mechanisms

while giving more detail than has previously been published (in particular, the scaling with amplitude, though considered in [16] and mentioned briefly in several works[17–19], has not previously been given a satisfactory analytical treatment or validated convincingly with simulations).

1. Velocity scaling

1.1. Physical picture

An isolated filament is, under the assumptions here, a density fluctuation comparable to or larger than the background in amplitude, extended along the magnetic field and with a monopolar structure perpendicular to it. The basic mechanism of filament motion is that there is a current source due to the inhomogeneity of the magnetic field which propels the filament, balanced by dissipation from, in the simple model considered here, drag due to the surrounding background plasma and from currents through the sheath where the magnetic field intersects the wall at the targets. This description is in some respects inspired by the 'equivalent circuit' picture[4, 20]. In contrast to the qualitative description in [4], here we consider drifts/currents only in the fluid model, rather than considering the particle drifts. In order to obtain simple expressions for the filament velocity, we reduce the problem to two dimensions by assuming zero variation parallel to the magnetic field and also assume that the filament reaches a steady state in which it travels at constant velocity. A more rigorous version of this argument, beginning from the plasma fluid equations, is encapsulated in the calculation given in Section 1.2.

Drive Due to the curvature of the magnetic field, represented by $\boldsymbol{\kappa} = -\hat{\boldsymbol{x}}/R_C$ where R_C is the radius of curvature, and the change in its magnitude with radius, $\nabla B = -B\hat{\boldsymbol{x}}/R_C$, the diamagnetic current $\boldsymbol{J}_{\text{dia}} = B^{-1}\nabla(nT)\times\hat{\boldsymbol{b}}$ has a non-zero divergence, as sketched in Figure 1. This divergence gives a current source whose strength is proportional to the pressure gradient in the direction perpendicular to $\boldsymbol{\kappa}$ and ∇B, which we will call $\hat{\boldsymbol{z}}$, and hence scales like $\Delta\delta_z^{-1}$ where Δ represents the filament amplitude (or, more accurately, some function of the amplitude, see Section 2.2) and δ_z is the typical scale in the $\hat{\boldsymbol{z}}$-direction. The total current source is then given by integrating over the volume of the filament and so scales like $L_\parallel\delta_x\delta_z\Delta/\delta_z = \Delta L_\parallel\delta_x$, where $L_\parallel$ is the length of the filament along the magnetic field, assumed the same as the connection length between the targets, and δ_x is the scale length in the $\hat{\boldsymbol{x}}$-direction (anti-parallel to $\boldsymbol{\kappa}$ and ∇B). In order to maintain quasineutrality, this current must be closed. Depending on the parameters of the filament, this may occur either through the polarisation current (giving rise to 'aerodynamic' drag) or the parallel current (giving rise to sheath current dissipation).

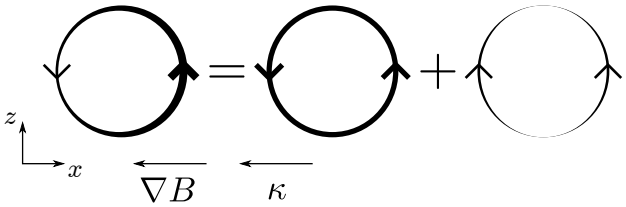

Figure 1. Diamagnetic current in a filament: The width of the line represents the magnitude of the current (integrated in the $\hat{\boldsymbol{b}}$-direction). The diamagnetic current (left) can be split into a divergence-free part (centre) and the remainder (right). This last, divergent part must be closed by parallel or polarisation currents and so provides the drive for filament motion

Aerodynamic drag When the current source closes through the polarisation current it results in a $\boldsymbol{J}\times\boldsymbol{B}$ force on the filament. We can estimate the total force by taking the net polarisation current to flow for a distance δ_z, so that the force scales like $\Delta L_\parallel\delta_x\delta_z$. The scaling is as if it were a body force (like, for example, gravity or buoyancy), but this is a mere coincidence arising from the combination of scaling of the current source and the mode of its action on the filament through $\boldsymbol{J}\times\boldsymbol{B}$. The dissipation, however, has a simpler physical picture; it is aerodynamic drag arising from the inertia of the the background plasma which must be displaced by the filament as it moves. Therefore the drag scales as the frontal area of the filament, $L_\parallel\delta_z$, and as the square of its velocity, V_{f}^2. Thus the propelling force and the drag balance when $V_{\text{f}} \sim \sqrt{\Delta\delta_x}$.

Sheath current dissipation When the current source closes through the parallel current it is regulated by the sheath boundary condition, (8), which determines the current that passes through the Debye sheath to the target plates. For small currents the sheath behaves as an ideal resistor, with current proportional to the electrostatic potential, ϕ. In steady state the potential is then proportional to the current source, so scales like $\Delta\delta_z^{-1}$. The

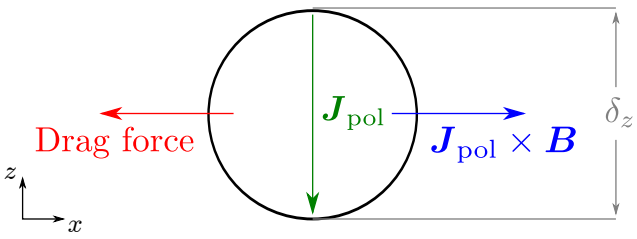

Figure 2. The forces acting on a filament in which the diamagnetic current closes through the polarisation current path

filament velocity is given by the $\boldsymbol{E} \times \boldsymbol{B}$ drift. Since the electric field generated is in the $\hat{\boldsymbol{z}}$-direction, the velocity scales as $V_{\mathrm{f}} \sim E_z \sim \phi/\delta_z \sim \Delta\delta_z^{-2}$.

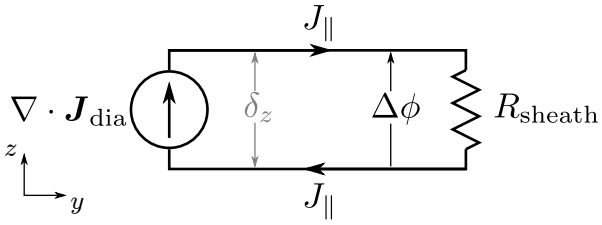

Figure 3. Equivalent circuit for a filament in which the diamagnetic current closes through the parallel current path

1.2. Scaling calculation

We use a coordinate system that takes $\hat{\boldsymbol{x}}$ in the 'radial' direction (anti-parallel to the magnetic field curvature and ∇B), $\hat{\boldsymbol{y}}$ along the magnetic field and $\hat{\boldsymbol{z}}$ in the binormal direction. We consider the steady motion of a coherent density structure, so that we neglect all time-variation except for the displacement of the filament, at constant velocity in the $\hat{\boldsymbol{x}}$-direction, $\boldsymbol{V}_{\mathrm{f}} = V_{\mathrm{f}}\hat{\boldsymbol{x}}$. We take the filament to be a monopolar density structure (possibly distorted, in the inertial regime), characterised by two length scales, δ_x and δ_z in the $\hat{\boldsymbol{x}}$- and $\hat{\boldsymbol{z}}$-directions, and an induced, dipolar potential structure. To aid visualisation of the configuration, the density and potential from a simulation (see Section 2) of a filament in the sheath current regime are shown in Figure 4. We assume cold ions and isothermal electrons, neglect electron inertia and use Bohm normalisation (as in [8], times are normalised to the ion cyclotron frequency $\Omega_{\mathrm{ci}} = eB_0/m_{\mathrm{i}}$, lengths to the hybrid Larmor radius $\rho_{\mathrm{s}} = c_{\mathrm{s}}/\Omega_{\mathrm{ci}}$, where $c_{\mathrm{s}} = \sqrt{T_{\mathrm{e}}/m_{\mathrm{i}}}$ is the sound speed, and electrostatic potential by T_{e}/e, with e the elementary charge, B_0 the magnetic field strength, m_{i} the ion mass and T_e the electron temperature; in addition densities are normalised to a typical value, usually the background density). Signs of gradients in scaling expressions are taken in the upper half-plane, e.g. $\nabla_z n \sim -n/\delta_z$.

The velocity scaling will follow from quasineutrality, $\nabla\cdot\boldsymbol{J} = 0$. As the total current is the sum of diamagnetic, polarisation and parallel contributions, $\boldsymbol{J} = \boldsymbol{J}_{\mathrm{dia}} + \boldsymbol{J}_{\mathrm{pol}} + \boldsymbol{J}_{\parallel}$, we now need to evaluate the divergence of each

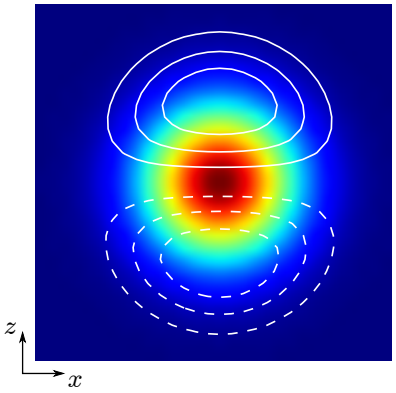

Figure 4. Density (colour-map) and potential (contours; solid for $\phi > 0$, dashed for $\phi < 0$) for a filament in the sheath regime, at maximum V_x

of these terms.

Diamagnetic current For cold ions, the diamagnetic current is due just to the electron diamagnetic velocity. Neglecting electron inertia and viscosity, the electron momentum equation is

$$0 = -\nabla n + n\nabla\phi + n\frac{\boldsymbol{V}_\mathrm{e}\times\boldsymbol{B}}{B_0}. \tag{1}$$

Taking the cross product with $\hat{\boldsymbol{b}}$ gives the perpendicular electron velocity with two contributions, the $\boldsymbol{E}\times\boldsymbol{B}$ and diamagnetic velocities: $\boldsymbol{V}_\mathrm{e} = \boldsymbol{V}_{E\times B} + \boldsymbol{V}_\mathrm{dia}$, with

$$n\boldsymbol{V}_\mathrm{dia} = -B_0\frac{\nabla n\times\hat{\boldsymbol{b}}}{B}. \tag{2}$$

Here we must not yet take $B = B_0$ (B_0 being the constant magnetic field used for normalisation) until we have taken its gradient in the divergence of the diamagnetic current:

$$\begin{aligned}\nabla\cdot\boldsymbol{J}_\mathrm{dia} &= B_0\nabla\cdot\left(\frac{\nabla n\times\hat{\boldsymbol{b}}}{B}\right)\\ &= -B_0\frac{\nabla n\cdot\nabla\times\hat{\boldsymbol{b}}}{B} - B_0\frac{\nabla B\cdot\nabla n\times\hat{\boldsymbol{b}}}{B^2}\\ &= 2\frac{\hat{\boldsymbol{z}}\cdot\nabla n}{R_\mathrm{C}} = -\hat{\boldsymbol{b}}\cdot\boldsymbol{g}\times\nabla n \sim -\frac{g}{\delta_z}\left(n-n_0\right),\end{aligned} \tag{3}$$

for a toroidal magnetic field $\boldsymbol{B} = \boldsymbol{e}_\phi/R$ at a major radius $R = R_\mathrm{C}$ (R_C denoting the radius of curvature of the magnetic field and $\boldsymbol{e}_\phi$ being the unit vector in the toroidal direction) much larger than the size of a filament and defining $\boldsymbol{g} = g\hat{\boldsymbol{x}} = \hat{\boldsymbol{x}}/R_\mathrm{C}$.

Polarisation current To evaluate the polarisation current contribution, we start from the total momentum equation (neglecting electron inertia)

$$\begin{aligned}\frac{\partial\boldsymbol{V}_\mathrm{i}}{\partial t} + \boldsymbol{V}_\mathrm{i}\cdot\nabla\boldsymbol{V}_\mathrm{i} &= \frac{1}{n}\boldsymbol{J}\times\hat{\boldsymbol{b}} - \frac{1}{n}\nabla n + \mu_\mathrm{i}\nabla_\perp^2\boldsymbol{V}_\mathrm{i}\\ &= \frac{1}{n}\boldsymbol{J}_\mathrm{pol}\times\hat{\boldsymbol{b}} + \mu_\mathrm{i}\nabla_\perp^2\boldsymbol{V}_\mathrm{i}.\end{aligned} \tag{4}$$

In the second line we have removed the diamagnetic contribution to $\boldsymbol{J}\times\hat{\boldsymbol{b}}$, which balances the pressure gradient exactly. This part includes the effects both of inertia, as discussed in Section 1.1, on the left of (4), and also the viscosity, μ_i. Assuming that the filament moves coherently with velocity $\boldsymbol{V}_\mathrm{f}$, then in the filament frame (defined by $\{\tilde{x},\tilde{z}\} = \{x - V_\mathrm{f}t, z\}$ and in which $\tilde{\boldsymbol{V}} = \boldsymbol{V} - \boldsymbol{V}_\mathrm{f}$) $\partial\tilde{\boldsymbol{V}}_\mathrm{i}/\partial t = 0$ and the momentum equation becomes

$$\tilde{\boldsymbol{V}}_\mathrm{i}\cdot\tilde{\nabla}\tilde{\boldsymbol{V}}_\mathrm{i} = \frac{1}{n}\boldsymbol{J}_\mathrm{pol}\times\hat{\boldsymbol{b}} + \mu_\mathrm{i}\tilde{\nabla}_\perp^2\tilde{\boldsymbol{V}}_\mathrm{i}. \tag{5}$$

We use this equation to estimate $\boldsymbol{J}_\mathrm{pol}$. Since the polarisation current does not flow in from the boundaries, it is clear that only the $\hat{\boldsymbol{z}}$-component can close the diamagnetic current divergence (since the divergent part of the diamagnetic current moves charge in the positive $\hat{\boldsymbol{z}}$-direction, the current closing it must move charge back in the negative $\hat{\boldsymbol{z}}$-direction). Taking the $\hat{\boldsymbol{x}}$-component of (5),

$$J_{\mathrm{pol},z} = -n\tilde{\boldsymbol{V}}_\mathrm{i}\cdot\tilde{\nabla}\tilde{V}_{\mathrm{i},x} + \mu_\mathrm{i}\tilde{\nabla}_\perp^2\tilde{V}_{\mathrm{i},x}.$$

For a configuration with a symmetric monopole in density and symmetric dipole in potential (as in Figure 4), it is clear that $J_{\mathrm{pol},z}$ (which is odd under $\hat{\boldsymbol{x}}$-reflection) cannot close the divergence of the diamagnetic current (which is even under $\hat{\boldsymbol{x}}$-reflection). Therefore a quasi-stationary state cannot be symmetric; it may instead have, as shown in Figure 5, a fairly symmetric potential dipole, but a distorted density structure, which is largely displaced to the right side of the potential dipole. As far as the scaling calculation is concerned, this makes no difference to the magnitudes, but indicates that the appropriate signs to take in the estimation of $J_{\mathrm{pol},z}$ are those in the region of largest density (while $\boldsymbol{V}_\mathrm{i}$ remains symmetric, the current is weighted by the density and so is larger in this region, which therefore gives the dominant contribution), namely in the upper half-plane between the $\phi = 0$ line and the maximum of ϕ, and on the right-hand side of the dipole (and when the inertia terms dominate $n\tilde{V}_{\mathrm{i},x}\nabla_x\tilde{V}_{\mathrm{i},x}$ must be larger than $n\tilde{V}_{\mathrm{i},z}\nabla_z\tilde{V}_{\mathrm{i},x}$ in steady state so that $J_{\mathrm{pol},z}$ is in the right direction). Thus we find

$$\begin{aligned}J_{\mathrm{pol},z} \sim &-\frac{n}{\delta_x}\tilde{V}_{\mathrm{i},x}^2 + \frac{n}{\delta_z}\tilde{V}_{\mathrm{i},z}\tilde{V}_{\mathrm{i},x}\\ &-\mu_\mathrm{i}\left(\frac{1}{\delta_x^2}+\frac{1}{\delta_z^2}\right)n\tilde{V}_{\mathrm{i},x}.\end{aligned} \tag{6}$$

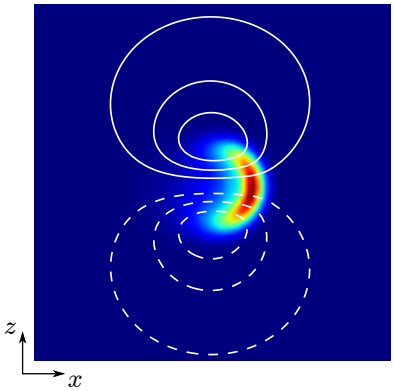

Figure 5. Density (colour-map) and potential (contours; solid for $\phi > 0$, dashed for $\phi < 0$) for a filament in the inertial regime, at maximum V_x

We can estimate $\tilde{V}_{\mathrm{i},z}$ from the density equation, which in the filament frame is

$$\nabla \cdot (n\tilde{\boldsymbol{V}}) = 0$$

$$\Rightarrow V_{\mathrm{i},z} \sim \frac{\delta_z}{\delta_x} V_{\mathrm{i},x}$$

and estimating the characteristic magnitude of $\tilde{V}_{\mathrm{i},x} \sim V_\mathrm{f}$, (6) becomes

$$\nabla_z J_{\mathrm{pol},z} \sim -\frac{n}{\delta_x \delta_z} V_\mathrm{f}^2 - \frac{\mu_\mathrm{i}}{\delta_z}\left(\frac{1}{\delta_x^2} + \frac{1}{\delta_z^2}\right) n V_\mathrm{f}. \tag{7}$$

Parallel current Linearising the sheath boundary condition,

$$J_\parallel\big|_\mathrm{sheath} = \pm n_\mathrm{sheath}\left(1 - e^{-\phi|_\mathrm{sheath}}\right) \approx \pm n\phi \tag{8}$$

and integrating over y,

$$\int dy\, \nabla \cdot \boldsymbol{J}_\parallel \approx 2n\phi.$$

Since the filament velocity is approximately the central $\boldsymbol{E} \times \boldsymbol{B}$ velocity of the filament (in the lab frame), we can further estimate $V_\mathrm{f} \sim \phi/\delta_z$ and hence

$$\int dy\, \nabla \cdot \boldsymbol{J}_\parallel \sim n\delta_z V_\mathrm{f} \tag{9}$$

Velocity scalings So finally, charge conservation

$$\nabla \cdot \boldsymbol{J} = 0$$

$$-\nabla \cdot \boldsymbol{J}_\mathrm{pol} = \nabla \cdot \boldsymbol{J}_\mathrm{dia} + \nabla \cdot \boldsymbol{J}_\parallel$$

gives, integrating over y and using (3), (7) and (9),

$$\underbrace{\frac{V_\mathrm{f}^2}{\delta_x}}_{\text{inertia}} + \underbrace{\mu_\mathrm{i}\left(\frac{1}{\delta_x^2} + \frac{1}{\delta_z^2}\right) V_\mathrm{f}}_{\text{viscosity}} \sim \underbrace{g\frac{(n-n_0)}{n}}_{\text{drive}} - \underbrace{\frac{1}{L_\parallel}\delta_z^2 V_\mathrm{f}}_{\substack{\text{sheath}\\ \text{dissipation}}}. \tag{10}$$

We can find several asymptotic limits by balancing each of the dissipative terms against the diamagnetic drive:

- sheath current regime

$$V_\mathrm{f} \sim \frac{L_\parallel g}{\delta_z^2}\frac{(n-n_0)}{n} \tag{11}$$

valid for

$$\delta_z^2\sqrt{\delta_x} \gg L_\parallel \sqrt{g\frac{(n-n_0)}{n}} \tag{12}$$

$$\text{and} \quad \frac{\delta_x^2\delta_z^4}{(\delta_z^2+\delta_x^2)} \gg L_\parallel \mu_\mathrm{i} \tag{13}$$

- inertial regime

$$V_{\rm f} \sim \sqrt{\delta_x g \frac{(n-n_0)}{n}} \tag{14}$$

valid for

$$\delta_z^2 \sqrt{\delta_x} \ll L_\parallel \sqrt{g \frac{(n-n_0)}{n}} \tag{15}$$

$$\text{and} \quad \frac{\delta_x^{\frac{3}{2}} \delta_z^2}{(\delta_x^2+\delta_z^2)} \gg \frac{\mu_{\rm i}}{\sqrt{g\frac{(n-n_0)}{n}}} \tag{16}$$

- viscous regime

$$V_{\rm f} \sim \frac{\delta_x^2 \delta_z^2 g}{(\delta_x^2+\delta_z^2)\,\mu_{\rm i}} \frac{(n-n_0)}{n} \tag{17}$$

valid for

$$\frac{\delta_x^2 \delta_z^4}{(\delta_z^2+\delta_x^2)} \ll L_\parallel \mu_{\rm i} \tag{18}$$

$$\text{and} \quad \frac{\delta_x^{\frac{3}{2}} \delta_z^2}{(\delta_x^2+\delta_z^2)} \ll \frac{\mu_{\rm i}}{\sqrt{g\frac{(n-n_0)}{n}}} \tag{19}$$

We have a sequence of different scalings as the filament width varies, with viscosity dominating for the narrowest filaments, sheath dissipation dominating for the widest filaments and inertia dominating at an intermediate scale, if the other parameters leave a sufficient window for this to happen (if $\mu_{\rm i} \ll L_\parallel^{3/5}(g(n-n_0)/n)^{4/5}$ for circular filaments). Interestingly, the velocity depends on δ_x but not δ_z in the inertial regime and conversely on δ_z but not δ_x in the sheath current regime. The latter point was noted in the seminal paper [21], in the case without background plasma where a separable solution exists, but seems to have been neglected since then.

2. Comparison with simulations

We have used two dimensional simulations to validate the scalings derived in Section 1.2. The equations used represent a filament assumed to have negligible variation along the magnetic field; closure is given by integrating the three-dimensional system over the parallel direction to give equations for the density and vorticity

$$\frac{dn}{dt} = \hat{\boldsymbol{b}} \cdot \boldsymbol{g} \times (n\nabla\phi - \nabla n) + \frac{n\left(1-e^{-\phi}\right)}{L_\parallel} + \mu_n \nabla_\perp^2 n \tag{20}$$

$$\frac{d\Omega}{dt} = -\frac{1}{n}\hat{\boldsymbol{b}} \cdot \boldsymbol{g} \times \nabla n + \frac{\left(1-e^{-\phi}\right)}{L_\parallel} + \mu_{\rm i} \nabla_\perp^2 \Omega \tag{21}$$

$$\Omega = \frac{1}{n}\nabla \cdot (n \nabla_\perp \phi) \approx \nabla_\perp^2 \phi \tag{22}$$

with $d/dt = \left(\partial/\partial t + \hat{\boldsymbol{b}} \cdot \nabla\phi \times \nabla\right)$ and, as before, $\boldsymbol{g} = g\hat{\boldsymbol{x}}$. The Boussinesq approximation (neglecting gradients of n) is used in (22) to simplify the Laplacian inversion. The dimensionless parameters used are $L_\parallel = 11000$, $g = 2.5 \times 10^{-3}$, $\mu_n = 1.5 \times 10^{-5}$ and $\mu_{\rm i} = 4 \times 10^{-4}$; for this theoretical study the dissipative parameters have been reduced by a factor of 100 (except in Appendix A) compared to those used in [8], based on the expressions in [22], in order to separate the transitions from viscous to inertial regimes and from inertial to sheath regimes so that the inertial scaling can be separately observed. Filaments are initialised as Gaussian density fluctuations with elliptical contours, tilted at an angle α to the $\hat{\boldsymbol{x}}$-direction, on a constant background,

$$n(t=0) = n_0\left(1 + A\exp\left(-\frac{\hat{x}^2/\epsilon + \epsilon\hat{z}^2}{\delta^2}\right)\right) \tag{23}$$

where A is the amplitude of the filament, ϵ is the ratio of the lengths of the axes of the ellipse, δ is the geometric mean of the lengths of the axes, $\hat{x} = x\cos\alpha + z\sin\alpha$ and $\hat{z} = z\cos\alpha - x\sin\alpha$. The diagram in figure 6 shows the configuration with the corresponding length scales, in the $\hat{\boldsymbol{x}}$- and $\hat{\boldsymbol{z}}$-directions respectively,

$$\delta_x = \delta\sqrt{\frac{\epsilon}{\left(\cos^2\alpha + \epsilon^2\sin^2\alpha\right)}} \tag{24}$$

$$\delta_z = \delta\sqrt{\frac{\epsilon}{\left(\epsilon^2\cos^2\alpha + \sin^2\alpha\right)}}, \tag{25}$$

which appear in the velocity scaling above. Filament velocities are measured as the maximum velocity of the centre of mass of the density above background, i.e. $n - n_0$, in the $\hat{\boldsymbol{x}}$-direction. These simulations, as well as the three dimensional ones in Section 3, have been implemented using BOUT++[23, 24].

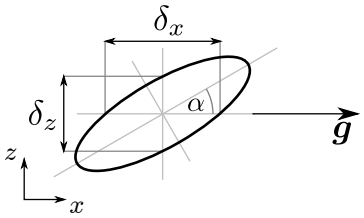

Figure 6. Schematic showing sizes and orientation of a tilted, elliptical filament cross-section

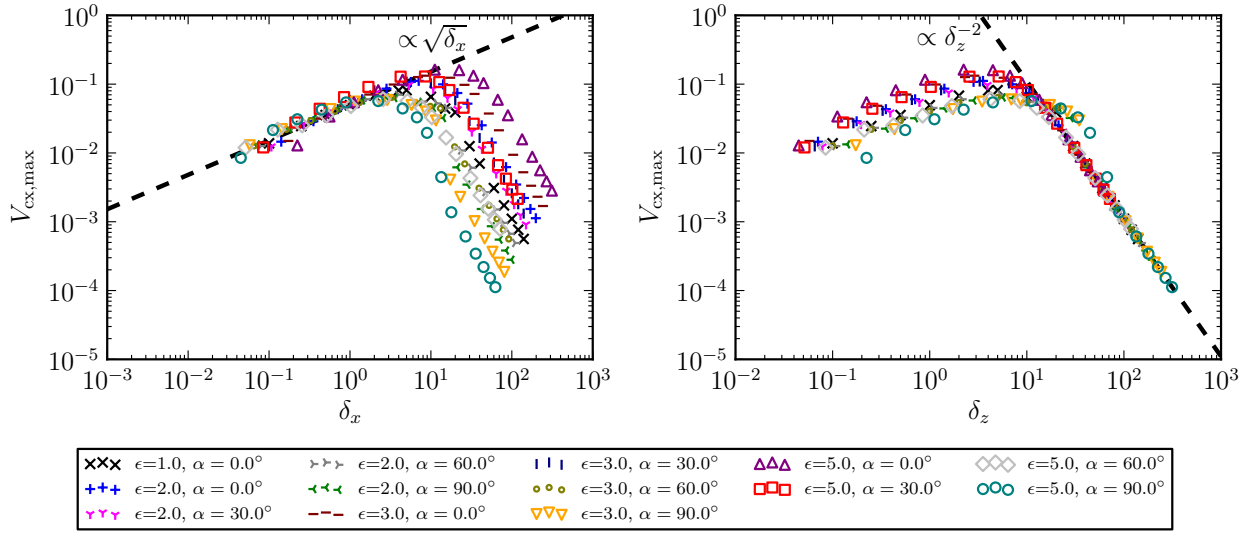

Figure 7. Inertial scaling vs. δ_x (left) and sheath current scaling vs. δ_z (right) with $A = 4$ for several values of ϵ and α

2.1. Scaling with size and shape

The results of a scan in width δ, ellipticity ϵ and inclination α, at constant amplitude $A = 4$, are shown in Figure 7. For four different ϵ and four different α, scanning δ results in a region of $\sqrt{\delta_x}$ scaling, corresponding to the inertial regime, and a region of δ_z^{-2} scaling corresponding to the sheath current regime. Moreover, although we have a three parameter space, $\{\delta, \epsilon, \alpha\}$, of filament sizes and shapes, a single combination (δ_x in the inertial regime and δ_z in the sheath current regime) entirely determines the filament velocity, at a particular amplitude (the effect of amplitude will be discussed in Section 2.2); this is evident from Figure 7 since all the points, for any ϵ and α (in the region where they follow $\sqrt{\delta_x}$ or δ_z^{-2} scaling) have not only the same gradient but also the same absolute magnitude.

The results for $\epsilon = 3$, $\alpha = 90°$ and $\epsilon = 5$, $\alpha = 90°$ exceed the δ_z^{-2} scaling for $\delta_z \approx 20 - 50$. This is due to the non-linearity of the sheath boundary condition which is included in the simulations, but not in the scaling. The maximum value of the potential is $\phi \approx 1.3$ at $\delta_z \approx 35$ for $\epsilon = 3$ and $\phi \approx 1.2$ at $\delta_z \approx 22$ for $\epsilon = 5$, so it makes sense that the deviation of $\exp(-\phi)$ from its linearised form is noticeable here. The effect of the non-linearity is to decrease the magnitude of the negative lobe of potential and increase the positive lobe. However, the enhancement of the positive lobe must be larger in order to allow the same magnitude, j_0, of current through the sheath: $|\phi_+| / |\phi_-| = -\ln(1 - j_0) / \ln(1 + j_0) > 1$. The overall effect is therefore to increase the filament velocity, since the increase from the positive lobe outweighs the decrease from the negative lobe, resulting in a larger E_z.

The trend lines are $V \approx 4.8 \times 10^{-2}\sqrt{\delta_x}$ for the inertial scaling and $V \approx 11\delta_z^{-2}$ for the sheath scaling. These intersect at $\delta_z^{4/5}\delta_x^{1/5} \approx 8.8$ whereas (12) and (15) suggest a crossover at $\delta_z^{4/5}\delta_x^{1/5} \approx 14.6$ for these parameters, in good agreement up to the order unity factors which are not fixed by analytical scaling arguments. (16) predicts that the crossover from inertial to viscous regime is mostly below the widths in the scan; the largest limit as a function of δ_x is for the $\epsilon = 5$, $\alpha = 0°$ case, where (16) evaluates to $\delta_x \gg 0.27$ and indeed the first point in this series (at $\delta_x \approx 0.22$) is indeed slightly below the $\sqrt{\delta_x}$ scaling, indicating that the viscosity is beginning to have an effect; scaling in the viscous regime is examined briefly in Appendix A, using larger dissipation parameters.

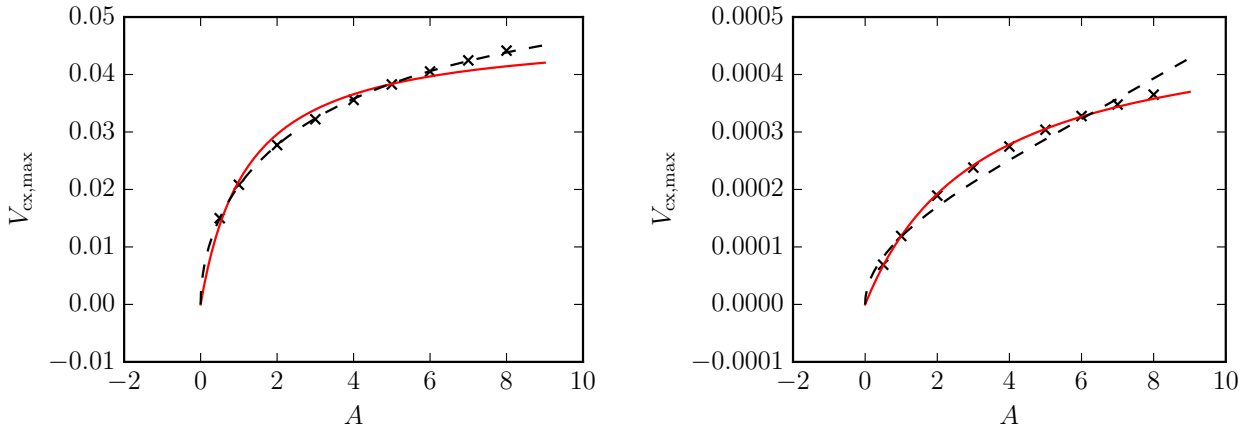

Figure 8. Amplitude scaling in the inertial regime, $\delta_x = \delta_z = 0.5$, (left) and in the sheath current regime, $\delta_x = \delta_z = 200$, (right). The solid red line shows the fitted linear ansatz, (26), and the dashed black line shows the fitted square-root ansatz, (27)

2.2. Amplitude scaling

From the maximum fluctuation amplitude $A = \max\left[(n - n_0)/n_0\right]$ we may estimate $\nabla_z(n - n_0) \sim An_0/\delta_z$, but we need to find a representative value of n to estimate $n^{-1}\nabla_z(n - n_0)$. We find, by fitting the simulation results, that the appropriate value is neither the maximum, $n \sim (1 + A)n_0$ nor the background $n \sim n_0$, but rather an intermediate value $n \sim (1 + \beta A)n_0$, where $0 < \beta < 1$. β corresponds to some point on the density profile at a distance $\tilde{\delta}_z$: $\beta = \exp(-\tilde{\delta}_z^2/\delta_z^2)$. Then V_f as a function of A with all other parameters held constant is, from (11), (14) and (17),

$$V_\mathrm{f} \propto \frac{A}{1 + \beta A} \qquad \text{sheath current or viscous regimes} \tag{26}$$

$$V_\mathrm{f} \propto \sqrt{\frac{A}{1 + \beta A}} \qquad \text{inertial regime} \tag{27}$$

if the representative value of n is found at the same relative position, $\tilde{\delta}_z/\delta_z$ for any A. This does indeed seem to be the case, as illustrated in Figure 8. For an amplitude scan with $\delta_x = \delta_z = 0.5$, which is in the inertial regime, (27) (residual 2.0×10^{-4}) gives a much better fit than (26) (residual 2.1×10^{-2}) and gives $\beta \approx 0.12$. Conversely, for an amplitude scan with $\delta_x = \delta_z = 200$, which is in the sheath current regime, (26) (residual 1.8×10^{-3}) gives a much better fit than (27) (residual 7.6×10^{-2}) and gives $\beta \approx 0.31$. This conclusion holds also when varying the ellipticity, see Appendix B.

Comparing this to previous work: the most detailed consideration of amplitude dependence is Kube and Garcia[16], where the scaling analysis starts from the vorticity equation and finds similar results to those given here, except that they assume a form equivalent to setting $\beta = 1$ which prevents them from finding a quantitative, analytical amplitude scaling (their fit coefficients vary with amplitude, whereas here we have only a single, constant coefficient, β, to be derived from simulations); Angus et al.[6] give, albeit briefly, a derivation along very similar lines to the one here, but neglect the amplitude dependence of the drive; Theiler et al.[19] in contrast use an interchange instability growth rate to estimate $\partial/\partial t \sim \gamma_\mathrm{interchange}$, and find a linear scaling with amplitude of the filament velocity in the inertial regime (which is contradicted here, emphasising that it is the non-linear, advective, term that is relevant); their derivation in [19] follows Garcia et al.[17, 25], but there the 'ideal interchange rate' is defined, without explanation, as

$$\gamma = \left(\frac{g}{\ell}\frac{\Delta\theta}{\Theta}\right)^{1/2}$$

(where g corresponds to our g, ℓ to $L_\parallel$, $\Delta\theta$ is the fluctuation amplitude and Θ is the background density) which includes an amplitude dependence giving a square-root scaling of the filament velocity in the inertial regime.

3. Three-dimensional validation

Here the normalised background density in the two dimensional simulations was set to $n_0 \approx 1.48$ to be consistent with the (source-driven) background used for the three-dimensional simulations, which normalise to the equilibrium density at the sheath entrance. The amplitude was set to a lower value than in the two dimensional case, $A = 2$, to avoid the possibility of drift wave instabilities playing a role in the three dimensional

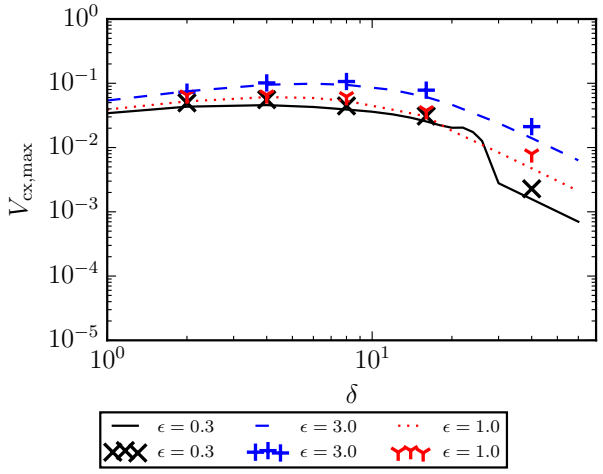

Figure 9. Comparison of 2D (lines) and 3D (markers) results for $A = 2$ and several ϵ

simulations. For more details on the equations used in and implementation of three dimensional simulations, see [8]. The three-dimensional filaments were initialised with no variation in the parallel direction, in order to correspond to the two dimensional calculation as closely as possible; investigation of really 'three-dimensional' effects due to parallel gradients is left for future work. Figure 9 shows that the three-dimensional simulations follow the two dimensional trends closely.

The velocity of three dimensional filaments in the sheath current regime is slightly larger than the corresponding two dimensional ones. We attribute this to the variation in the background density: since this decreases near the sheath, the potential needed to drive the same sheath current is slightly increased and it follows that the filament velocity must then increase slightly.

The bump on the $\epsilon = 1/3$ curve between $\delta = 20$ and $\delta = 30$, the part most affected by the non-linearity of the boundary condition (see Section 2.1), is due to the eventual fragmentation and subsequent acceleration of the filaments. In other words, it is due to their ceasing to travel as coherent structures and so its investigation is a subject beyond the scope of this paper.

4. Discussion

A number of works[18, 19] have analysed filament motion by analogy with the theory of linear instabilities; this has been termed the 'blob correspondence principle'[18, 26]. Our analysis above shows that the picture is not quite so simple, the nature of the filaments as coherent, non-linear objects is important because the density and potential fields have fundamentally different structures, the density being a (possibly distorted) monopole and the potential being a dipole (see Figures 4 and 5), rather than the identical structures, up to a phase shift, that they have in the linear theory. This is particularly evident in the amplitude scaling (Section 2.2) where the parameters of the scaling depend on the relative scale lengths of the potential and density. Moreover, the nature of the physical processes involved in limiting filament velocity are clearer when considering the filament itself instead of analysing the governing equations by analogy or 'correspondence' to linear theory.

An interesting point to note is that the derivation of the scalings in Section 1.2 does not depend on whether or not the Boussinesq approximation, (22), is used. It therefore predicts that velocities of isolated filaments will not be affected much by the approximation, although their coherence, stability and interactions may well be.

5. Conclusions

We have given here the first calculation of SOL filament velocity to include the effect of the filament shape and have also clarified the role of the filament amplitude. The analytical scaling calculations have been extensively validated by two dimensional simulation results, and also compared (with good agreement) to three-dimensional simulations in which the filaments are initialised without parallel variation. Thus we now have a complete understanding of the mechanisms of filament propagation in the simple limit considered here. This understanding provides a solid foundation for the interpretation of filament motion in more complicated, more realistic models.

Acknowledgements

We would like to thank Prof. Steve Cowley for stimulating discussions which provided the initial impetus for the work described here. This work has been carried out within the framework of the EUROfusion Consortium and has received funding from the Euratom research and training programme 2014-2018 under grant agreement No 633053 and from the RCUK Energy Programme [grant number EP/I501045]. To obtain further information on the data and models underlying this paper please contact PublicationsManager@ccfe.ac.uk. The views and opinions expressed herein do not necessarily reflect those of the European Commission. This work used the ARCHER UK National Supercomputing Service (http://www.archer.ac.uk) under the Plasma HEC Consortium EPSRC grant number EP/L000237/1.

Appendix A. Viscous regime

For MAST relevant values of the dissipative parameters[8, 22], $\mu_n = 1.5 \times 10^{-3}$ and $\mu_\mathrm{i} = 4 \times 10^{-2}$, there is not a clear inertial regime with $\sqrt{\delta_x}$ scaling between the viscous and sheath current regimes, as we see in Figure A1. There is δ^2 scaling in the viscous regime, consistent with (17), but even though the dissipative parameters for MAST are relatively large (due to low magnetic field, high safety factor and high collisionality), pure δ^2 scaling is reached only for $\delta < 1$, i.e. for filaments narrower than the hybrid Larmor radius, ρ_s. Therefore the asymptotic viscous regime cannot be physically relevant, which is the reason that we do not pursue a more detailed characterisation here. However for these parameters, small filaments, $1 < \delta < 10$, are clearly affected (although not dominated) by viscosity.

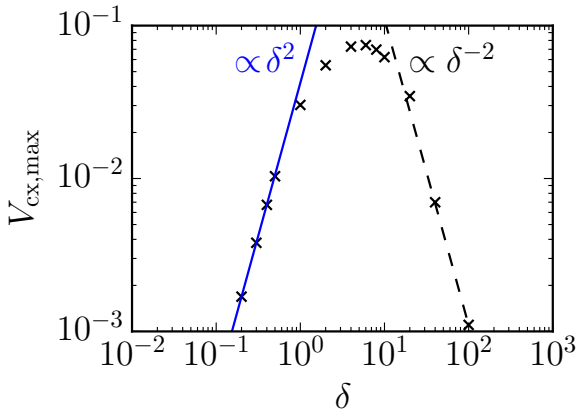

Figure A1. Scaling for circular filaments with amplitude $A = 4$ and using MAST relevant dissipative parameters

Appendix B. Amplitude scaling fits

δ_z	β	$\frac{\text{residual(sqrt)}}{\text{residual(lin)}}$
0.5/10	-0.05030	14.74
0.5/5	0.005967	0.9183
0.5/3	0.04802	0.1704
0.5/2	0.08022	0.03628
0.5	0.1244	0.009581
0.5×2	0.1479	0.01428
0.5×3	0.1440	0.02435
0.5×5	0.1271	0.1082
0.5×10	0.08299	0.4548

Table B1. Inertial regime: Comparison of (i) values of β inferred by least squares regression on the relative error between the ansatz (27) (square-root scaling) and filament velocities measured from simulations and (ii) ratio of residual for this regression to that for regression with the ansatz (26) (linear scaling), at $\delta_x = 0.5$ for several values of δ_z. Amplitudes used for the analysis were $A = 1, 1.5, 2, 3, 4, 5, 6, 7, 8$.
For extreme values of ellipticity the filament is no longer in the pure inertial regime. Both viscous and sheath current regimes have linear scaling, so the square-root fit is then less good.

δ_x	β	$\frac{\text{residual(lin)}}{\text{residual(sqrt)}}$
200/10	0.3105	0.02341
200/5	0.3110	0.02341
200/3	0.3111	0.02342
200/2	0.3113	0.02327
200	0.3113	0.02329
200×2	0.3109	0.02390
200×3	0.3108	0.02358
200×5	0.3109	0.02383
200×10	0.2333	0.06529

Table B2. Sheath current regime: Comparison of (i) values of β inferred by least squares regression on the relative error between the ansatz (26) (linear scaling) and filament velocities measured from simulations and (ii) ratio of residual for this regression to that for regression with the ansatz (27) (square-root scaling), at $\delta_z = 200$ for several values of δ_x. Amplitudes used for the analysis were $A = 1, 1.5, 2, 3, 4, 5, 6, 7, 8$.

References

[1] Ayed N B, Kirk A, Dudson B, Tallents S, Vann R G L, Wilson H R and the MAST team 2009 *Plasma Physics and Controlled Fusion* **51** 035016 URL http://stacks.iop.org/0741-3335/51/i=3/a=035016

[2] Boedo J A, Rudakov D L, Moyer R A, McKee G R, Colchin R J, Schaffer M J, Stangeby P G, West W P, Allen S L, Evans T E, Fonck R J, Hollmann E M, Krasheninnikov S, Leonard A W, Nevins W, Mahdavi M A, Porter G D, Tynan G R, Whyte D G and Xu X 2003 *Physics of Plasmas (1994-present)* **10**

[3] Myra J, Davis W, D'Ippolito D, LaBombard B, Russell D, Terry J and Zweben S 2013 *Nuclear Fusion* **53** 073013 URL http://stacks.iop.org/0029-5515/53/i=7/a=073013

[4] Krasheninnikov S, D'Ippolito D and Myra J 2008 *Journal of Plasma Physics* **74**(05) 679–717 ISSN 1469-7807 URL http://journals.cambridge.org/article_S0022377807006940

[5] D'Ippolito D A, Myra J R and Zweben S J 2011 *Physics of Plasmas (1994-present)* **18** 060501 URL http://scitation.aip.org/content/aip/journal/pop/18/6/10.1063/1.3594609

[6] Angus J R, Krasheninnikov S I and Umansky M V 2012 *Physics of Plasmas (1994-present)* **19** 082312 URL http://scitation.aip.org/content/aip/journal/pop/19/8/10.1063/1.4747619

[7] Walkden N R, Dudson B D and Fishpool G 2013 *Plasma Physics and Controlled Fusion* **55** 105005 URL http://stacks.iop.org/0741-3335/55/i=10/a=105005

[8] Easy L, Militello F, Omotani J, Dudson B, Havlíčková E, Tamain P, Naulin V and Nielsen A H 2014 *Physics of Plasmas (1994-present)* **21** 122515 URL http://scitation.aip.org/content/aip/journal/pop/21/12/10.1063/1.4904207

[9] Madsen J, Garcia O E, Stærk Larsen J, Naulin V, Nielsen A H and Rasmussen J J 2011 *Physics of Plasmas (1994-present)* **18** 112504 URL http://scitation.aip.org/content/aip/journal/pop/18/11/10.1063/1.3658033

[10] Ricci P and Rogers B N 2013 *Physics of Plasmas (1994-present)* **20** 010702 URL http://scitation.aip.org/content/aip/journal/pop/20/1/10.1063/1.4789551

[11] Militello F, Tamain P, Fundamenski W, Kirk A, Naulin V, Nielsen A H and the MAST team 2013 *Plasma Physics and Controlled Fusion* **55** 025005 URL http://stacks.iop.org/0741-3335/55/i=2/a=025005

[12] Tamain P, Ghendrih P, Bufferand H, Ciraolo G, Colin C, Fedorczak N, Nace N, Schwander F and Serre E 2015 *Plasma Physics and Controlled Fusion* **57** 054014 URL http://stacks.iop.org/0741-3335/57/i=5/a=054014

[13] Yu G Q and Krasheninnikov S I 2003 *Physics of Plasmas (1994-present)* **10**

[14] Dudson B D, Ayed N B, Kirk A, Wilson H R, Counsell G, Xu X, Umansky M, Snyder P B, LLoyd B and the MAST team 2008 *Plasma Physics and Controlled Fusion* **50** 124012 URL http://stacks.iop.org/0741-3335/50/i=12/a=124012

[15] Easy L, Militello F, N W, Omotani J and Dudson B 2015 *to be submitted to Physics of Plasmas*

[16] Kube R and Garcia O E 2011 *Physics of Plasmas (1994-present)* **18** 102314 URL http://scitation.aip.org/content/aip/journal/pop/18/10/10.1063/1.3647553

[17] Garcia O E, Bian N H, Naulin V, Nielsen A H and Rasmussen J J 2005 *Physics of Plasmas (1994-present)* **12** 090701 URL http://scitation.aip.org/content/aip/journal/pop/12/9/10.1063/1.2044487

[18] Myra J R and D'Ippolito D A 2005 *Physics of Plasmas (1994-present)* **12** 092511 URL http://scitation.aip.org/content/aip/journal/pop/12/9/10.1063/1.2048847

[19] Theiler C, Furno I, Ricci P, Fasoli A, Labit B, Müller S H and Plyushchev G 2009 *Phys. Rev. Lett.* **103**(6) 065001 URL http://link.aps.org/doi/10.1103/PhysRevLett.103.065001

[20] Russell D A, D'Ippolito D A, Myra J R, Nevins W M and Xu X Q 2004 *Phys. Rev. Lett.* **93**(26) 265001 URL http://link.aps.org/doi/10.1103/PhysRevLett.93.265001

[21] Krasheninnikov S 2001 *Physics Letters A* **283** 368 – 370 ISSN 0375-9601 URL http://www.sciencedirect.com/science/article/pii/S0375960101002523

[22] Fundamenski W, Garcia O, Naulin V, Pitts R, Nielsen A, Rasmussen J J, Horacek J, Graves J and contributors J E 2007 *Nuclear Fusion* **47** 417 URL http://stacks.iop.org/0029-5515/47/i=5/a=006

[23] Dudson B, Umansky M, Xu X, Snyder P and Wilson H 2009 *Computer Physics Communications* **180** 1467 – 1480 ISSN 0010-4655 URL http://www.sciencedirect.com/science/article/pii/S0010465509001040

[24] Dudson B D, Allen A, Breyiannis G, Brugger E, Buchanan J, Easy L, Farley S, Joseph I, Kim M, McGann A D, Omotani J T, Umansky M V, Walkden N R, Xia T and Xu X Q 2015 *Journal of Plasma Physics* **81**(01) ISSN 1469-7807 URL http://journals.cambridge.org/article_S0022377814000816

[25] Garcia O E, Bian N H and Fundamenski W 2006 *Physics of Plasmas (1994-present)* **13** 082309 URL http://scitation.aip.org/content/aip/journal/pop/13/8/10.1063/1.2336422

[26] Myra J R, Russell D A and D'Ippolito D A 2006 *Physics of Plasmas (1994-present)* **13** 112502 URL http://scitation.aip.org/content/aip/journal/pop/13/11/10.1063/1.2364858